SCIENCE CHINA
Technological Sciences

February 2010 Vol.53 No.2: 326–342
doi: 10.1007/s11431-009-0331-x

Forming limits under multi-index constraints in NC bending of aluminum alloy thin-walled tubes with large diameters

YAN Jing, YANG He*, ZHAN Mei & LI Heng

College of Materials Science and Engineering, State Key Laboratory of Solidification Processing, Northwestern Polytechnical University, Xi'an 710072, China

Received May 19, 2009; accepted July 13, 2009

With increasing diameters of aluminum alloy thin-walled tubes (AATTs), the tube forming limits, i.e. the minimum bending factors, and their predictions under multi-index constraints including wrinkling, thinning and flattening have been being a key problem to be urgently solved for improving tube forming potential in numerical control (NC) bending processes of AATTs with large diameters. Thus in this paper, a search algorithm of the forming limits is put forward based on a 3D elastic-plastic finite element (FE) model and a wrinkling energy prediction model for the bending processes under axial compression loading (ACL) or not. This algorithm enables to be considered the effects of process parameter combinations including die, friction parameters on the multi-indices. Based on this algorithm, the forming limits of the different size tubes are obtained, and the roles of the process parameter combinations in enabling the limit bending processes are also revealed. The followings are found: the first, within the appropriate ranges of friction and clearances between the different dies and the tubes enabling the bending processes with smaller bending factors, the ACL enables the tube limit bending processes after a decrease of the mandrel ball thickness and diameters; then, without considering the effects of the tube geometry sizes on the tube constitutive equations, the forming limits will be decided by the limit thinning values for the tubes with diameters smaller than 80 mm, while the wrinkling for the tubes with diameters no less than 80 mm. The forming limits obtained from this algorithm are smaller than the analytical results, and reduced by 57.39%; the last, the roles of the process parameter combinations in enabling the limit bending processes are verified by experimental results.

forming limit, NC tube bending, aluminum alloy thin-walled tubes with large diameters, multi-index constraints, finite element method

Citation: Yan J, Yang H, Zhan M, et al. Forming limits under multi-index constraints in NC bending of aluminum alloy thin-walled tubes with large diameters. Sci China Tech Sci, 2010, 53: 326–342, doi: 10.1007/s11431-009-0331-x

1 Introduction

As a kind of key lightweight components, aluminum alloy thin-walled tubes (AATTs) with larger diameters (tube diameters and wall thickness ratios>30) and smaller bending factors (ratios of bending radii to tube diameters) have opened up an attractive future for their wide applications in aerospace, aviation, automobile and related high technology industries. The rapid development of the above industries urgently requires research and development of advanced plastic forming technologies to enable the manufacture of the tube parts. Numerical control (NC) tube bending (Figure 1(a)), based on a rotary draw method, has become an advanced technology satisfying this requirement due to its many advantages such as efficient, economical, stable forming process, and easier to achieve digital precision forming process and enable the large quantity batch production [1, 2]. However, forming qualities in the NC bending processes of AATTs with large diameters are constrained by the multi-

*Corresponding author (email: yanghe@nwpu.edu.cn)

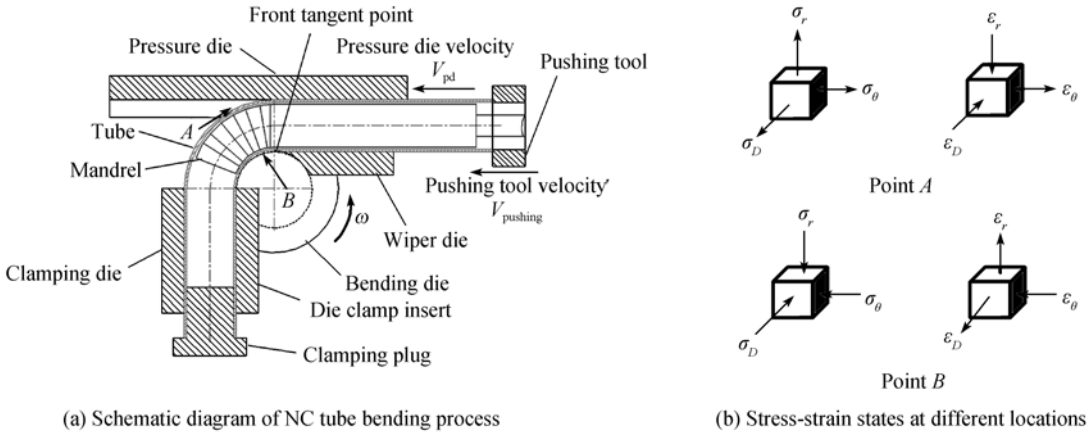

(a) Schematic diagram of NC tube bending process (b) Stress-strain states at different locations

Figure 1 Schematic diagram of an NC tube bending process and tube stress-strain states.

indices including wrinkling, thinning and flattening, and the control of the forming qualities in these processes has been a challenging problem with an increase of the diameters and a decrease of the bending radii.

As shown in Figure 1(b), in an NC bending process, a tube is subjected to the 3D tension stress on extrados and the 3D compression stress on intrados, respectively. This will lead to thinning on extrados and flattening in cross-section, and even wrinkling possibility on intrados. Especially, the wrinkling possibility would increase significantly with increasing the tube diameters and decreasing the bending factors. Thus, rigorous contacting conditions between the various dies and the tubes are usually applied to decrease the wrinkling possibilities in the bending processes of AATTs with larger diameters and smaller bending factors, but they will also easily lead to the excessive thinning and flattening of tubes. This will make it difficult to enable limit NC bending processes of AATTs with large diameters, because tube forming limits, i.e. the minimum bending factors, will be decided by multi-indices including the wrinkling, the thinning and the flattening. Thus, the forming limits and their predictions have become a key problem to be urgently solved for improving industrial application potential of these tubes. However, up to now, there have hardly been any sufficient studies reported in the literatures on such tube forming limits under the multi-index constraints.

Great efforts have been made for studying forming limits in sheet or tube metal forming processes respectively by analytical [3–8], experimental [9] and numerical simulation approaches [10–14]. The analytical approach is mainly based on plastic deformation mechanics or plastic instability theory, by which the relationships between the forming indices and the chosen parameters are established firstly, and then the limit parameters corresponding to the limit forming indices are taken as the forming limits, such as the limit stress or strain for the fracture or the wrinkling in the sheet forming processes [3, 4], the limit internal pressure and axial force for the wrinkling or the fracture in the tube hydro-forming processes [5] and the minimum bending radii for the wrinkling in the tube bending processes [6–8]. The experimental approach is based on an on-line measure of the limit parameters, e.g., the limit strain for the wrinkling in the sheet drawing forming processes is on-line measured, and then the wrinkling limit diagram is obtained [9]. The numerical simulation approach has been used to study the forming limits by the finite element (FE) analysis for the metal forming processes, e.g., the sheet limit drawing ratios for the fracture are investigated for the sheet hot drawing forming processes [10], and the minimum bending radii for the flattening are studied for the rectangle tube bending processes with rubber pad [13], etc.

As shown in Figure 1(a), the tube is covered by the various dies in the NC bending process and this process needs the various dies to perform in coordination, which makes it difficult to study the forming limits by the experimental approach. Wang et al. [6] and Yang et al. [7] obtained the minimum bending factors for the wrinkling in the tube bending processes based on an analytical wrinkling energy prediction model, respectively. In their studies, effects of friction and clearances between the different dies and the tubes on the wrinkling were not considered, and thus their methods are not appropriate for obtaining the ones in these NC bending processes of AATTs with large diameters under multi-die constraints. By adding the work into the wrinkling prediction model done by the interaction force between the dies and the tube, and by introducing the straight line segment of the compression zone into the critical wrinkling zone, Li et al. [14] modified the energy wrinkling prediction model and then studied the wrinkling prediction in the NC tube bending processes by combining this model with the rigid-plastic FE model. However, it was still difficult to simulate the contact conditions between the dies and the tube in the rigid-plastic FE model. Li et al. [8] also investigated the minimum bending factors analytically based on the modified wrinkling energy prediction model, and they obtained the band distributed wrinkling limit diagram only depending on tube diameters and wall thickness,

only depending on tube diameters and wall thickness, in which the effects of the process parameter combinations including the die, the friction and the velocity conditions on the wrinkling were not considered.

Considering the influences of die, friction and velocity conditions on forming processes, FE simulations based on an elastic-plastic dynamic explicit FE method can deal with various complicated forming problems effectively. Gu et al. [15] and Li et al. [16] established the dynamic explicit FE model for the NC bending processes of small diameter tubes (diameters<40 mm) based on the DYNAFORM and ABAQUS software environments, respectively. Li [17] studied the effects of the geometry and process parameters on the wrinkling for the stainless steel and aluminum alloy tubes with the small diameters by combining this explicit FE model with this modified wrinkling energy prediction model, suggesting the advantages of this combination method in studying the wrinkling characteristics and its prediction under multi-die constraints. But this wrinkling prediction method was not applied to the study of forming limits in the NC tube bending processes. Considering the characteristics of the bending processes of AATTs with large diameters, based on the ABAQUS software environment, Yang et al. [18] established the 3D elastic-plastic FE model and the wrinkling energy prediction model under multi-die constraints and validated the reliabilities of the models, respectively. Besides, in ref. [18], the combination of the established elastic-plastic explicit FE model with the wrinkling energy prediction model was also performed to enable the wrinkling characteristics in the bending processes to be predicted actually and efficiently, which has become a necessary base for studying the minimum bending factors of these different diameter AATTs.

Up to now, much research about the predictions of the minimum bending factors in the NC tube bending processes has been carried out mainly in investigating the small diameter tubes (diameters<30 mm). Because the effects of the process parameter combinations on the multi-indices in the bending processes have not been considered effectively, the obtained minimum bending factors are larger than the experimental results. Thus, it is necessary to obtain the minimum bending factors under the multi-index constraints, including the wrinkling, the thinning and the flattening, for realizing optimization designs of the dies and improving the tube forming potential in the NC bending processes of AATTs with large diameters.

In this paper, a search algorithm of the minimum bending factors under the multi-index constraints is put forward based on a 3D elastic-plastic FE model and a wrinkling energy prediction model for these bending processes of AATTs with large diameters under axial compression loading (ACL) or not. This algorithm can consider effectively the effects of process parameter combinations including die, friction conditions on the multi-indices in these bending processes with small bending factors. Based on this algorithm, the minimum bending factors of the different size tubes and the roles of the clearances and friction between the different dies and the tubes, the mandrel ball thickness and diameters, and the ACL in enabling these limit bending processes are obtained.

2 Research methodology

2.1 3D Elastic-plastic FE model under multi-die constraints

FE modeling for NC bending processes of AATTs with large diameters involves three types of nonlinearity: material, contact and geometry nonlinearity. The material nonlinearity in these processes is ascribed to the tube material elastic-plastic behaviors. The contact nonlinearity is evident in these bending processes because of the complex and changing dynamic contact between the tubes and the seven different dies including the pushing tool exerting ACL, the wiper die, the pressure die, the clamping die, the bending die, the mandrel and the plug, as shown in Figure 1(a). The geometry nonlinearity behaviors in these bending processes include the large displacement and rotation, the flattening, the wrinkling and the post-bulking of these tubes. In order to effectively analyze these nonlinearity behaviors, the elastic-plastic dynamic explicit FE algorithm on the ABAQUS software environment is chosen for simulating these tube bending processes.

In the dynamic explicit FE algorithm, a mass scaling factor can be used to decrease FE analysis time, but it can not be set too large in order to not increase inertial force of an FE simulation system excessively lest leading to poor simulation results. The effects of the die inertial force on the simulation system of these NC bending processes of AATTs with large diameters are larger than on the tubes with small diameters, thus the mass scaling of the dies is not considered in the FE modeling of these bending processes.

Figure 2 shows a representative FE model for these bending processes. In this model, the tube is a deformable body, and the forming dies including the pressure die, the bending die, the clamping die, the wiper die, the mandrel with one or more flexible balls, the clamping plug and the pushing tool are simplified as rigid bodies in order to improve computational efficiency.

With an increase of the tube diameter, the tube wall thickness is relatively much smaller than the dimensions in the tube circumferential and tangential directions, so the tube has much more evidently thin shell structure feature. Four-node doubly curved thin shell elements considering reduced integration and hourglass control are used to discretize the tube in order to simulate the large deformation and rotation and finite membrane strain in the bending processes [19]. The number of the simulation elements of large size tubes changes from 15000 to 33000. The rigid body surfaces of dies are discretized by 4-node 3D bilinear

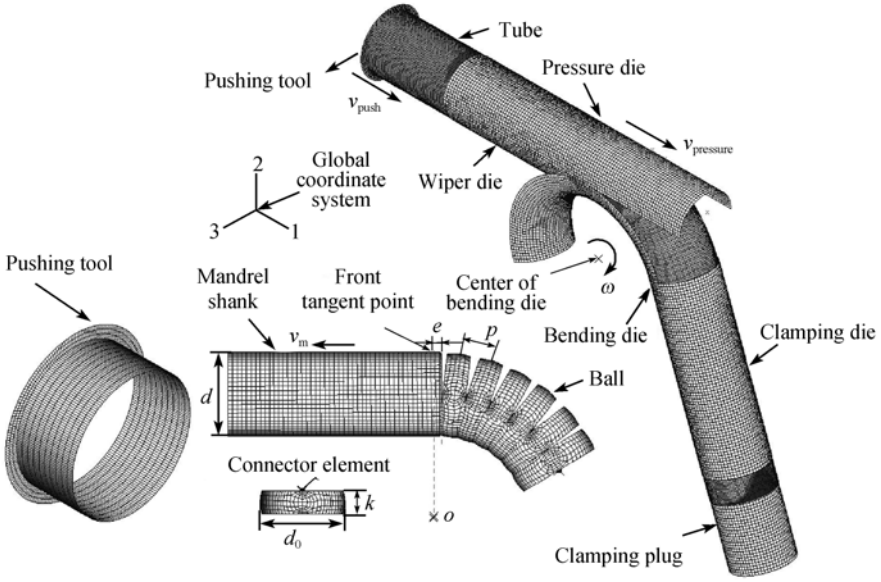

Figure 2 A representative finite element model.

quadrilateral rigid elements. The link between the different mandrel balls is modeled by a "connector element". The maximum rotation range p (Figure 2) of each mandrel ball is set in the properties of the "connector element".

The material model used in the simulation is an isotropic, homogeneous, elastic-plastic material following von-Mises yield criterion, with isotropic work hardening. Without the Bauschinger effects and the effects of tube geometrical sizes on the constitutive equations taken into account, the mechanical properties of the tube (5052O) were obtained from the uniaxial tensile test of the specimens cut along the longitudinal direction of the tube. The isotropic strain hardening of flow stress of tubes is defined as $\bar{\sigma} = 341.02\bar{\varepsilon}^{0.16526}$. The tube density is 2700 kg/m^3, the Poisson's ratio 0.3, and the Young's modulus 63 GPa.

As there is a relative slide between the different dies and the tubes, the Coulomb friction model is used to describe the friction between them, as shown in the following equation:

$$\tau_{crit}=\mu\sigma_n, \tag{1}$$

where μ ($0<\mu<0.5$) is known as the coefficient of friction and τ_{crit} is the critical shear stress, at which sliding of the surfaces starts as a fraction of the contact pressure, σ_n, between the surfaces [19]. Because the yield stress of aluminum alloy tube is smaller than that of the stainless steel, the extreme value of friction coefficient for aluminum alloy tube bending will be also smaller.

There is no relative slide between the tubes and the clamping dies, or the claming plugs in the bending processes, thus a "small-sliding formulation" is used to simulate the interactions between them in order to improve the computational efficiency. Conversely, a "finite-sliding formulation" is used to simulate the interactions between the tubes and the other dies in order to simulate effectively the tube large deformation and rotation in the contacting processes. Besides, contacting constraint conditions between the dies and the tubes in the simulations are that the nodes on the tube deformed surfaces must not penetrate the rigid die surfaces. A "penalty contact algorithm" is used to achieve these constraint conditions between the tubes and the mandrels, while a "kinematic contact algorithm" for the ones between the tubes and the other dies.

The established FE model for these NC bending processes of AATTs with large diameters has been verified by the experiment in ref. [18].

2.2 Forming indices for NC tube bending processes

In this paper, the tube wrinkling possibility is described by the maximum wrinkling factor, $I_w=T/U_{min}$, in which U_{min} is the minimum wrinkling energy of the tube compression zones, and T is the work done by the external force. The wrinkling occurrence is judged by the limit wrinkling value, $T/U_{min}\geqslant 1$. The computational method of the maximum wrinkling factor and its validation have been studied in ref. [18].

The tube thinning is described by the maximum thinning ratio I_t as follows:

$$I_t=(t-t_0)/t\times 100\%, \tag{2}$$

where t is initial wall thickness of tube, and t_0 is wall thickness at the thinnest point along the tube extrados. The excessive thinning is judged by the limit thinning values, $I_t\geqslant 22\%$, which is the material extension ratio.

The tube flattening is described as follows by the maximum ovality I_d:

$$I_d=(D-D')/D\times 100\%, \tag{3}$$

where D is the tube diameter before bending and D' is the tube diameter along the bending radius direction after bending, as shown in Figure 3. The excessive flattening is

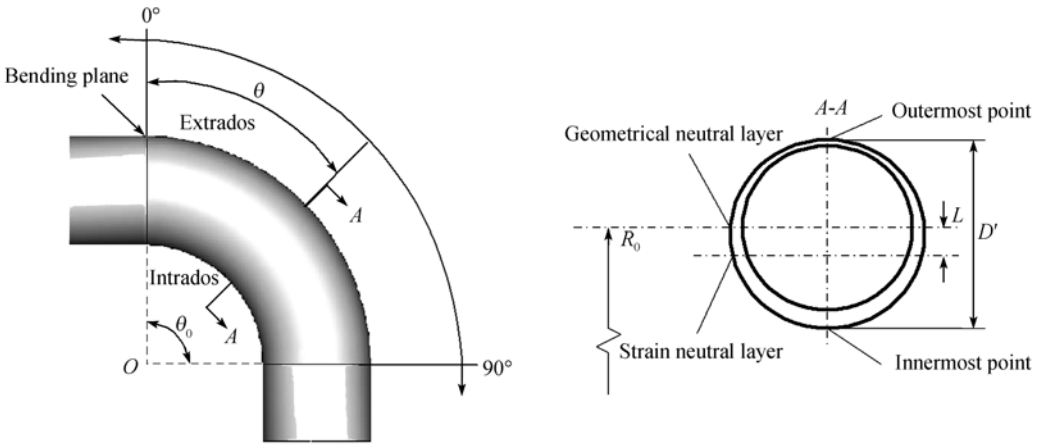

Figure 3 Measurement locations of obtained results.

judged by the limit flattening values, $I_d \geqslant 5\%$, satisfying the aircraft application demands.

2.3 Research methodology for forming limits of AATTs with large diameters

2.3.1 Definition of forming limits of NC tube bending with multi-die constraints

The minimum bending factors of AATTs with large diameters are decided by the three forming indices, i.e., I_w for wrinkling, I_t for thinning, and I_d for flattening as follows:

$$(R_0 / D)_{\min} = \phi(I_w, I_t, I_d). \tag{4}$$

The three forming indices are influenced by tube geometry (D/t, R_0/D), material (m) and process parameter combinations (f, c), respectively, and relationships between them are

$$\begin{cases} I_w = \varphi(m, D/t, R_0/D, f, c), \\ I_t = \varphi'(m, D/t, R_0/D, f, c), \\ I_d = \varphi''(m, D/t, R_0/D, f, c), \end{cases} \tag{5}$$

where m is material parameters including strength coefficient k, work-hardening exponent n, etc., D is tube diameter, t is tube wall thickness, R_0 is bending radius, f is friction parameters including friction between various dies and tubes, c is die parameters including clearances between various dies and tubes, mandrel parameters, and pushing tools.

According to eqs. (4) and (5), given m and D/t, for each process parameter combination $(f, c)^{(i)}$ (i indicates the number of these parameter combinations), the relationships between the R_0/D and these three indices can be established respectively by the FE model for the NC bending processes of AATTs with large diameters, and then the critical bending factors, i.e. $(R_0/D)^{(i)}_{cw}$ based on the wrinkling, $(R_0/D)^{(i)}_{ct}$ the thinning, and $(R_0/D)^{(i)}_{cd}$ the flattening, can be obtained by the limit index values. With the bending factors larger than the maximum critical bending factors, $\{(R_0/D)^{(i)}_{cw}, (R_0/D)^{(i)}_{ct}, (R_0/D)^{(i)}_{cd}\}^{(i)}_{max}$, and the corresponding process parameter combinations, $(f, c)^{(i)}$, the forming qualities for the bending processes will be acceptable. The minimum bending factor is the smallest one in all the maximum critical bending factors corresponding to the different process parameter combinations, i.e., $\{\{(R_0/D)^{(i)}_{cw}, (R_0/D)^{(i)}_{ct}, (R_0/D)^{(i)}_{cd}\}^{(i)}_{max}\}_{min}$. The optimum process parameter combination corresponding to the minimum bending factor is also determined. If the maximum critical bending factor corresponding to the process parameter combination, $(f, c)^{(i+1)}$, is smaller than $(f, c)^{(i)}$, it can be believed that the $(f, c)^{(i+1)}$ enables the tube NC bending processes with smaller bending factors.

2.3.2 Determination of appropriate ranges of process parameter combinations

According to eq. (5), given m, D/t, and R_0/D, the appropriate ranges of process parameter combinations can be determined. Figure 4 shows a determination method of the appropriate ranges. Fibonacci sequence of number [20] is also used in Figure 4 and shown in the following equation:

$$\begin{cases} F_0 = F_1 = 1, \\ F_{k'+1} = F_{k'} + F_{k'-1}, \ k' = 1, 2, \ldots. \end{cases} \tag{6}$$

A virtual multi-index orthogonal experiment $L_{27}(3^{13})$ is firstly executed by the FE modeling based on the changes of the clearances and friction between the various dies and the tubes. Then, the experimental results are measured by I_w, I_t, and I_d, respectively, and the clearances and friction between the various dies and the tubes corresponding to the minimum forming indices are decided, which can be used as one limit end point of these ranges.

In order to determine the other limit end point of these ranges precisely, the initial ranges of each parameter in the process parameter combinations are firstly determined according to the effects of the different parameters on these three forming indices. In the initial ranges of the process parameter combinations, each parameter is changed based

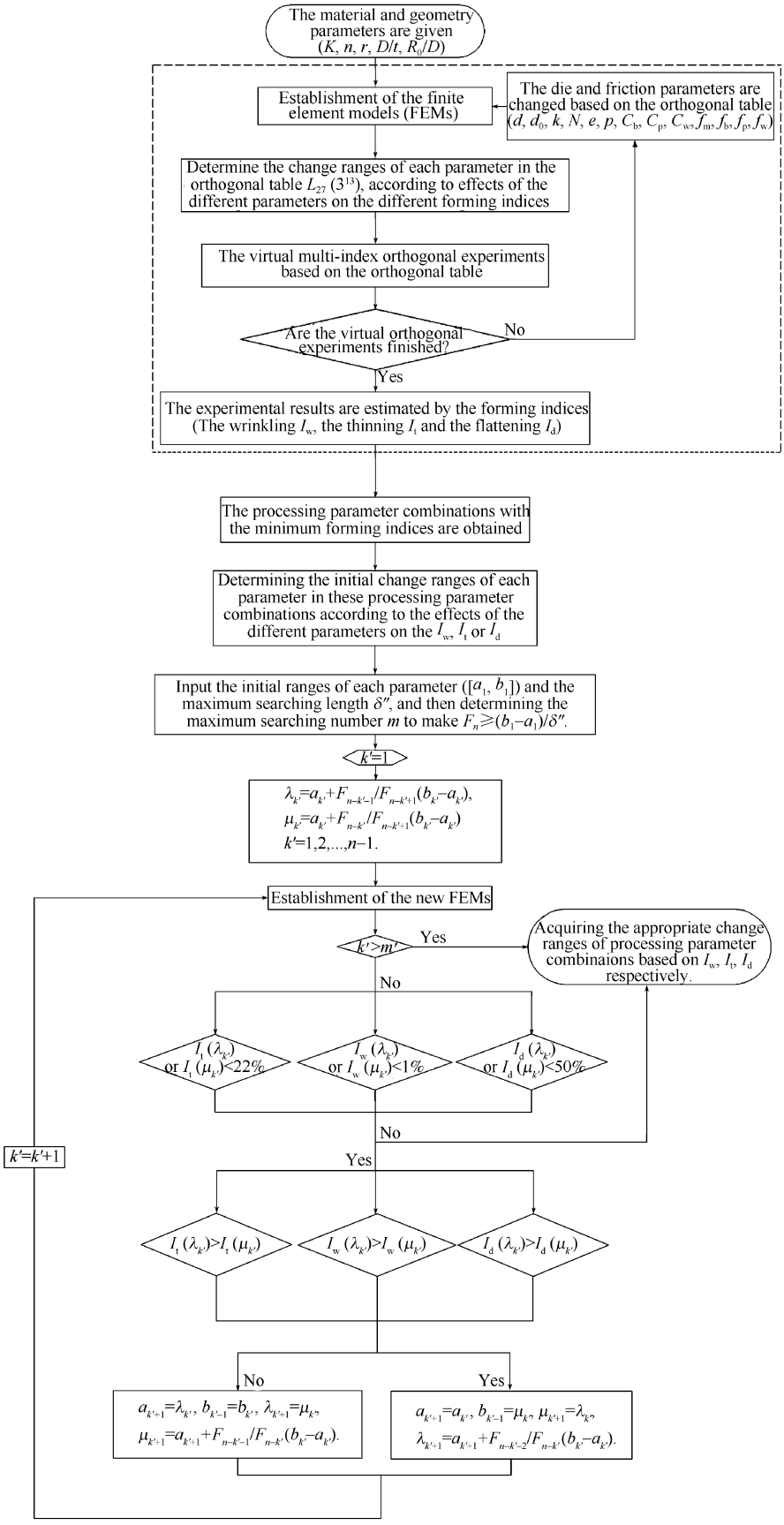

Figure 4 Determination method of appropriate ranges of process parameter combinations (The die and friction parameters in the figure are described in Tables 1 and 2).

Table 1 Friction parameter ranges in the different interfaces

Contact interfaces	Friction coefficient μ
Tube outside surface vs. clamping die	>0.60
Tube outside surface vs. wiper die, f_w	0.05–0.06
Tube outside surface vs. pressure die, f_p	0.25–0.30
Tube outside surface vs. bending die, f_b	0.25–0.30
Tube inside surface vs. clamping plug	0.25–0.30
Tube inside surface vs. mandrel with balls, f_m	0.05–0.06
Ball vs. ball	0.05–0.10

Note: The pressure die, the bending die and the clamping plug are unlubricated in the bending processes with μ of 0.25–0.3; the wiper die, and the mandrel with one or more balls are lubricated with μ of 0.05–0.06.

on Fibonacci search algorithm [20] in order to guarantee the search precision, and these simulation results corresponding to these different process parameter combinations can be obtained by the FE analysis for these bending processes. If I_w, I_t or I_d reaches the limit value, the corresponding process parameter combination can be decided, and used as the other limit end point of the ranges of the process parameter combinations based on the corresponding forming index. Thus, these three ranges of the process parameter combinations based on these three forming indices can be decided respectively, and the appropriate ranges of the process parameter combinations are the common ones of these three combination ones.

2.3.3 Searching algorithm of forming limits under multi-index constraints

Figure 5 shows a searching algorithm of the minimum bending factors of AATTs with large diameters. This algorithm enables the considerations of effects of process parameter combinations on these three forming indices including I_w, I_t and I_d in these NC tube bending processes. In this algorithm, given the tube material parameters, m, the geometry ones, $(D/t)^{(k)}$, and the initial bending factors, $(R_0/D)^{(0)}_{min}$ ($(R_0/D)^{(0)}_{min}<2$ in this study), the appropriate ranges of process parameter combinations are decided based on this method shown in Figure 4, which enables these bending processes under smaller bending factors and further the searching algorithm efficiency to be improved. If all the forming indices are less than the limit values within the obtained ranges of process parameter combinations, then decrease the bending factors; otherwise increase the bending factors. The change increment of the bending factors, ΔR, is set as 0.1 in order to improve the efficiency and precision of the searching algorithm. The smaller the bending factors, the smaller the appropriate ranges of the process parameter combinations. With changing the bending factors, the process parameter combinations, $(f^{(j)}, c^{(j)})$, will also be changed along the directions of decreasing the forming indices in these obtained ranges ($j \leqslant j_{max}$, in which j_{max} is the number of the process parameter combinations), according to the effects of different process parameters on these three forming indices. After the iterations of the above searching processes, the relationships between the bending factors and these three different forming indices for these different size tubes are established, respectively, based on which the critical bending factors, the minimum ones and the process parameter combinations corresponding to the different bending factors can be also determined, respectively.

Table 2 Die parameter ranges

Parameter	Value		
Tube diameter, D (mm)	70	80	100
Wall thickness, t (mm)	1	1	1
Bending radius, R_0 (mm)	105	120	170
Mandrel diameter, d (mm)	67.50–67.75	77.50–77.75	97.87–97.90
Ball diameter, d_0 (mm)	67.10–67.70	77.10–77.70	97.10–97.70
Thickness of ball, k (mm)	16–25	18–27	24–28
Number of balls, N	4	4	4
Extension length of mandrel, e (mm)	5–7	5–7	5–7
Final bending angle, θ_0 (rad)	$\pi/2$	$\pi/2$	$\pi/2$
Pitch between balls, p (mm)	19	22	41
Assembling clearance of pressure die, C_p (mm)	0.10–0.15	0.10–0.15	0.10–0.15
Assembling clearance of wiper die, C_w (mm)	0.15–0.20	0.15–0.20	0.13–0.17
Assembling clearance of bending die, C_b (mm)	0.10–0.15	0.10–0.15	0.10–0.15

Note: The cavity tolerances of pressure dies and wiper dies are set as 0–0.05 mm and the ones of bending dies 0.10–0.15 mm.

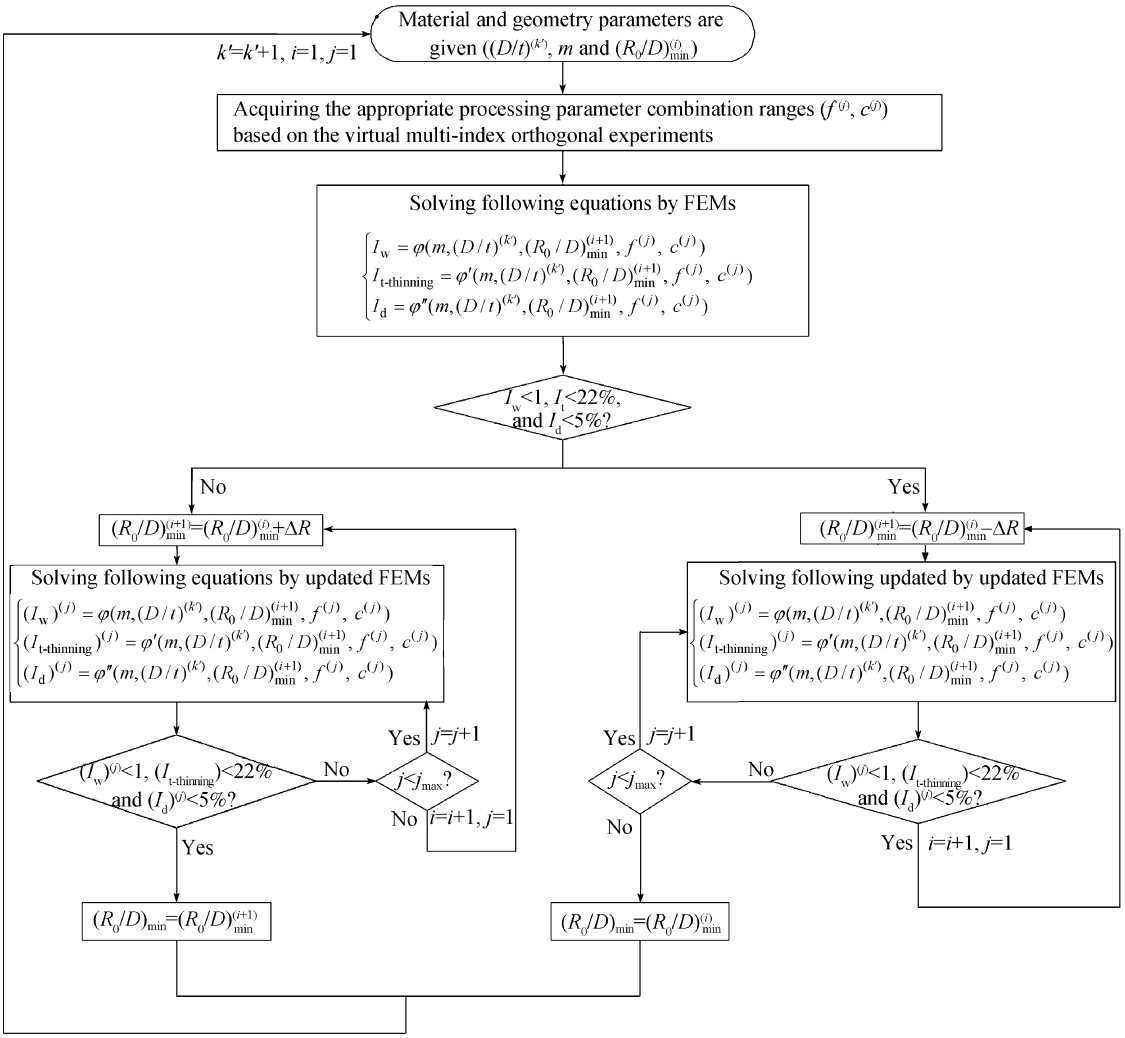

Figure 5 Determination method of forming limits under multi-index constraints.

3 Results and discussions

3.1 Effects of clearances and friction on critical bending factors

The die and friction parameter combination ranges for these bending processes with small bending factors (R_0/D <2) are obtained from the method shown in Figure 4 and listed in Tables 1 and 2.

Figure 6 shows the simulation results for Table 3, which are the limit end points of the parameter combination ranges shown in Tables 1 and 2. It can be found that the forming qualities of the different size tubes are all smaller than the limit values.

Figure 7 shows the effects of the clearances and friction between the various dies and the tubes on the wrinkling, the thinning and the flattening. From Figure 7, it can be found that both the thinning and flattening degrees corresponding to the clearances and friction between the different dies and the tubes shown in Table 3 are the smallest. Thus, the process parameter combinations corresponding to the minimum bending factors can be acquired from the parameter combinations shown in Table 3.

The contacting effects between the dies and the tubes can be measured by the clearances, the friction, and the contacting areas between them, or only by the clearances and the frictions for the same size tubes, i.e. the smaller the clearances or the larger the friction, the larger the contacting effects. From Figures 7(a) and (b), it can be found that with increasing the contacting effects between the pressure die and the tube or decreasing between the mandrel and the tube, the tube thinning degree will decrease, leading to the decrease of the tube critical bending factor based on the thinning. From Figures 7(c) and (d), it can be found that with increasing the contacting effects between the bending die and the tube or decreasing between the mandrel and the tube, the tube flattening degree will decrease, leading to the decreases of the critical bending factor based on the flattening. From Figures 7(e) and (f), it can be found that with increasing the contacting effects between the tube and the mandrel or the bending die, or decreasing between the pressure die

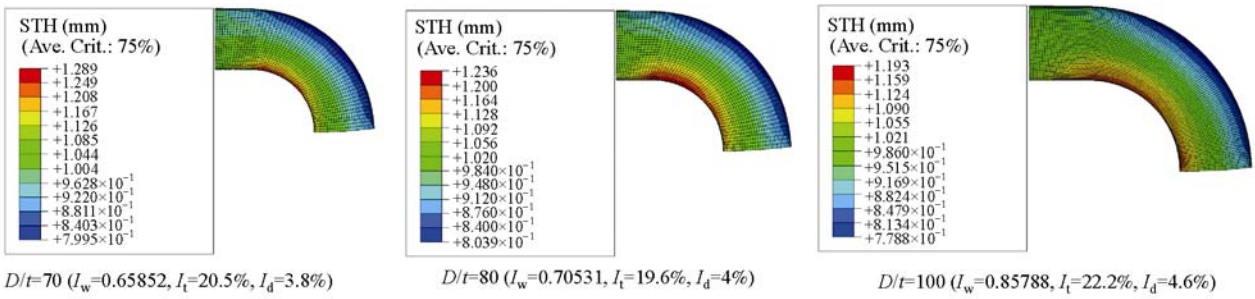

Figure 6 Simulation results of different size tubes.

Table 3 Process parameter combinations for simulations

Parameter	Value		
Tube diameter, D (mm)	70	80	100
Wall thickness, t (mm)	1	1	1
Bending radius, R_0 (mm)	105	120	170
Mandrel diameter, d (mm)	67.75	77.75	97.90
Ball diameter, d_0 (mm)	67.70	77.70	97.70
Thickness of ball, k (mm)	16	18	24
No. of balls, N	4	4	4
Extension length of mandrel, e (mm)	7	7	7
Assembling clearance of pressure die, C_p (mm)	0.15	0.15	0.15
Assembling clearance of wiper die, C_w (mm)	0.15	0.15	0.17
Assembling clearance of bending die, C_b (mm)	0.10	0.10	0.10
Tube outside surface vs. wiper die, f_w	0.05	0.05	0.05
Tube outside surface vs. pressure die, f_p	0.30	0.30	0.30
Tube outside surface vs. bending die, f_b	0.30	0.30	0.30
Tube inside surface vs. mandrel with balls, f_m	0.05	0.05	0.05

Note: The cavity tolerances of pressure dies and wiper dies are set as 0 mm and the ones of bending dies 0.1 mm

and the tube, the tube wrinkling possibility will decrease for the tube with larger D/t, leading to the decrease of the critical bending factor based on the wrinkling.

Based on the process parameter combinations shown in Table 3, for the tubes with the D/t of 70, 80, and 100, the effects of the clearance and friction parameters on the critical bending factors are studied. In Figure 8, the clearances between the mandrel shanks and the tubes are measured by the mandrel shank diameters. Figure 8(a) shows that for the larger mandrel ball thickness (k/d_0={0.36, 0.35, 0.34}) and the smaller mandrel shank diameters ($\boldsymbol{d}$={67.50 mm, 77.50 mm, 97.50 mm}), with decreasing the friction between the bending dies and the tubes, the tube critical bending factors based on both the wrinkling and the thinning will increase, and the wrinkling ones are larger than the thinning and flattening. This is because that the decreases of the mandrel shank diameters or friction between the bending dies and the tubes will increase the tube wrinkling possibilities. Besides, the parameters in Figure 8(a) cannot achieve the bending processes with the small bending factors, and the bending factors increase by 150%; the larger the D/t, the larger the above effects. It can be found from Figure 8(b) that for the smaller mandrel ball thickness (k/d_0={0.23, 0.23, 0.24}), if the mandrel shank diameters are kept unchanged ($\boldsymbol{d}$={67.75 mm, 77.75 mm, 97.90 mm}), the friction conditions between the bending dies and the tubes have the great influences on the critical bending factors only for the tubes with the D/t>80. For the tubes with the D/t<80, when the clearances between the mandrel shanks and the tubes are less than 0.6 mm, the critical bending factors based on the thinning are larger than the wrinkling with decreasing the mandrel diameters; but when the clearances $\geqslant$0.6 mm, the critical bending factors based on the wrinkling are larger than the thinning.

Under these optimum clearance and friction parameter combinations shown in Table 3, the roles of the mandrel ball thickness, the ball diameters and the ACL in enabling the limit bending processes of the tubes with the D/t of 70, 80 and 100 can be studied and further the tube minimum bending factors can also be obtained. The change ranges of the mandrel ball thickness and diameters are listed in Table 4. The ACL is exerted by the pushing tools, whose velocities in the simulations are the same as the assistant velocities of the pressure dies.

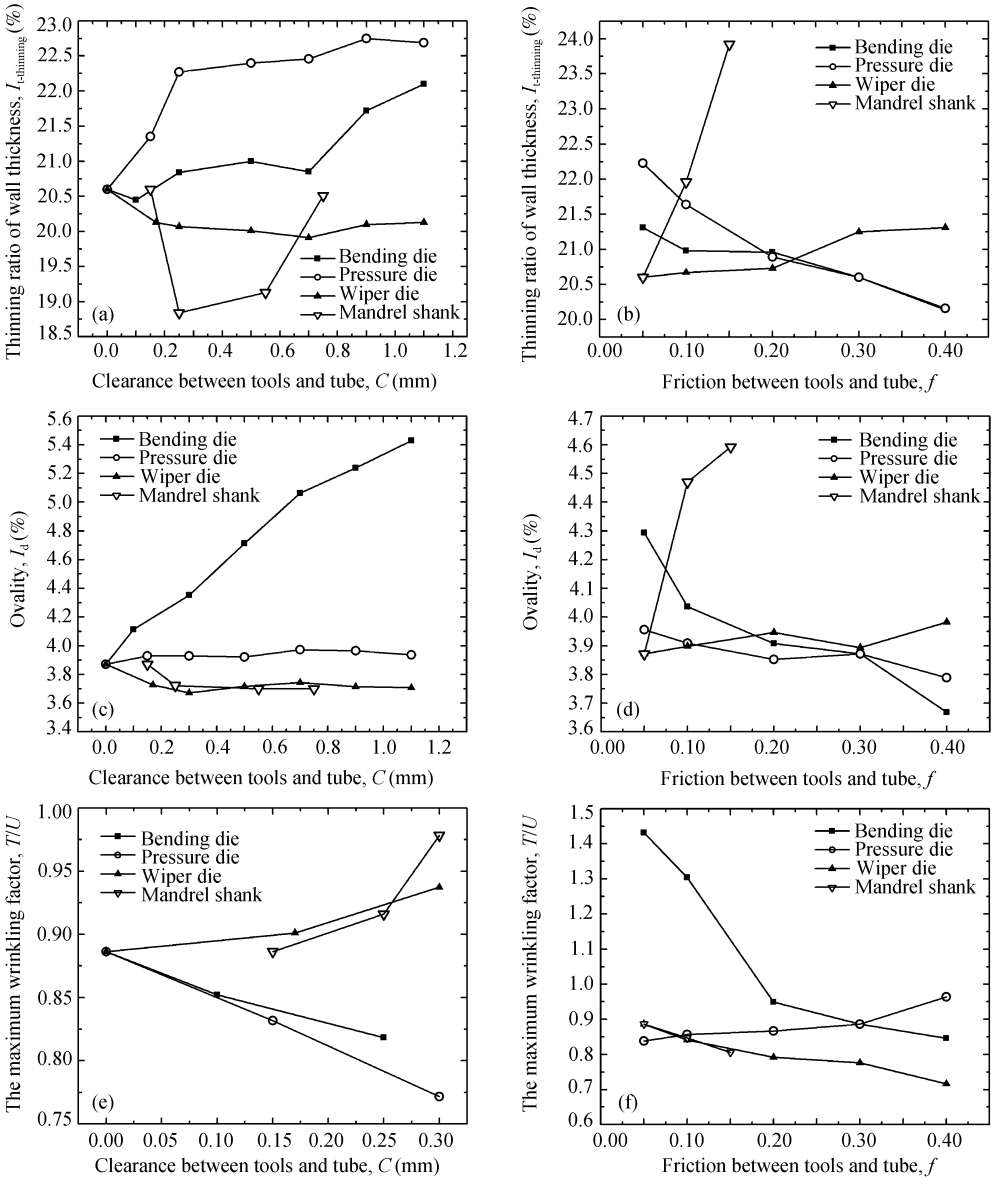

Figure 7 Effects of clearance and friction on different forming indices. (a) Effects of clearances on thinning (D/t=70); (b) effects of friction on thinning (D/t=70); (c) effects of clearances on flattening (D/t=70); (d) effects of friction on flattening (D/t=70); (e) effects of clearances on wrinkling (D/t=100); (f) effects of friction on wrinkling (D/t=100).

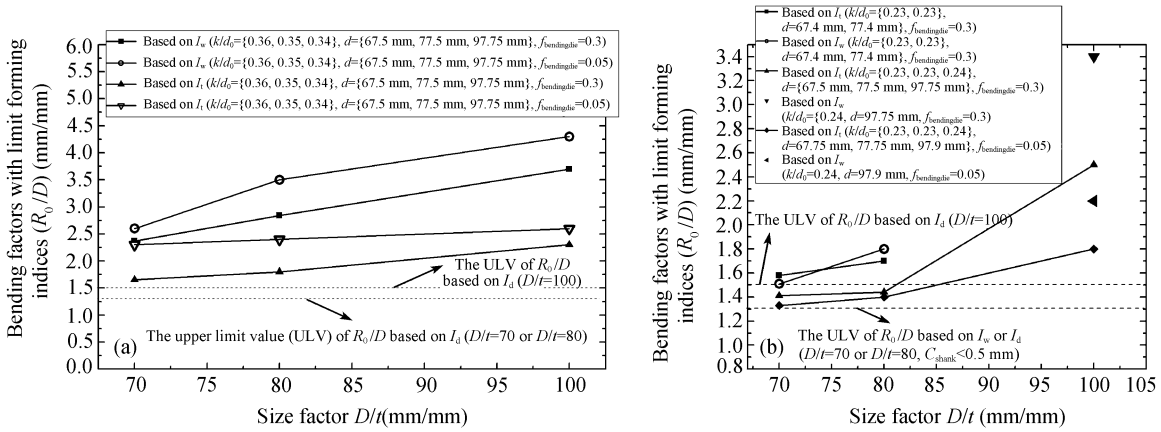

Figure 8 Effects of clearances and friction on critical bending factors. (a) k/d_0={0.36, 0.35, 0.34}; (b) k/d_0={0.23, 0.23, 0.24}.

Table 4 Change ranges of mandrel parameters

D/*t*	*k* (mm)	d_0 (mm)
70	{16,20,25}	{67.7,67.5,67.1}
80	{18,22,27}	{77.7,77.5,77.1}
100	{24,28,33}	{97.7,97.5,97.1}

3.2 Effects of mandrel ball thickness on critical bending factors

3.2.1 Effects of mandrel ball thickness on multi-indices

Figure 9 shows the effects of the mandrel ball thickness on the multi-indices under the different bending factors. It can be found from Figure 9 that with increasing *D*/*t* or decreasing bending factors, the increase of the mandrel ball thickness will lead to the large increases of both the tube wrinkling possibilities (Figure 9(a)) and thinning degrees (Figure 9(b)); the smaller the bending factors, the larger the above effects. But as shown in Figure 9(c), its increase will also lead to the decreases of tube flattening degrees, and the maximum ovality of all the tubes is still less than 5% with changing the mandrel ball thickness, because the tubes with the large *D*/*t* are not sensitive to the flattening.

3.2.2 Effects of mandrel ball thickness on the maximum critical bending factors

Figure 10 shows the tube critical bending factors corresponding to the different mandrel ball thickness obtained from Figure 9. It can be found that without changing the mandrel ball diameters, the larger the mandrel ball thickness, the larger the critical bending factors based on both the wrinkling and the thinning; the larger the *D*/*t*, the larger the effects of the mandrel ball thickness. For the tubes with *D*/*t*<80, the critical bending factors based on the thinning are larger than on the wrinkling and flattening, while for the tube with *D*/*t* of 100, the ones based on the wrinkling are larger than the others with increasing the mandrel ball thickness. Thus, with smaller *D*/*t*, the tube maximum critical bending factors will be based on the thinning, which are not sensitive to the change of the mandrel ball thickness; with increasing mandrel ball thickness and *D*/*t*, the ones will be based on the wrinkling.

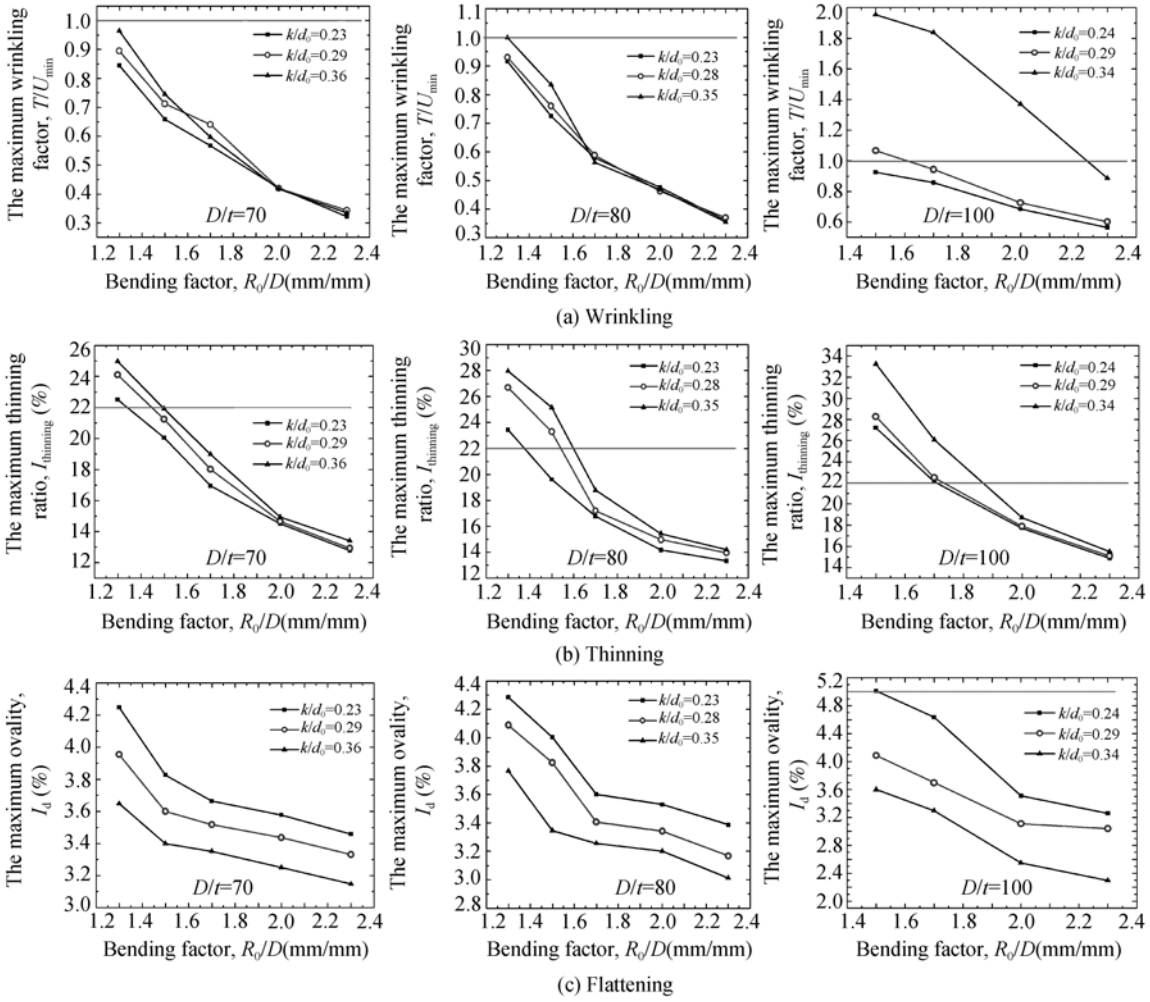

Figure 9 Effects of mandrel ball thickness on different forming indices.

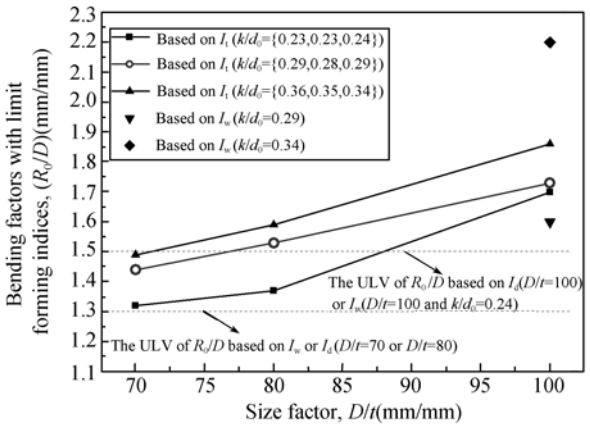

Figure 10 Effects of mandrel ball thickness on critical bending factors.

3.3 Effects of mandrel ball diameters on critical bending factors

3.3.1 Effects of mandrel ball diameters on multi-indices

Figure 11 shows the effects of the mandrel ball diameters on the multi-indices under the different bending factors. In Figure 11, the mandrel ball diameters are measured by the clearances between the mandrel balls and the tubes (C_{ball} (mm)), and the small ball thickness is used, i.e. $\boldsymbol{k}$={16 mm, 18 mm, 24 mm}, whose wrinkling possibilities are small. It can be found that from Figure 11, the changes of the mandrel ball diameters have the smaller influences on the tube wrinkling than the other indices under the different bending factors; the smaller the mandrel ball diameters, the smaller the tube thinning degrees and the larger the flattening; the larger the D/t, the smaller the mandrel ball diameter effects.

3.3.2 Effects of mandrel ball diameters on the maximum critical bending factors

Figure 12 shows the tube critical bending factors corresponding to the different mandrel ball diameters obtained from Figure 11. It can be found that the decreases of the mandrel ball diameters will lead to the decreases of the critical thinning bending factors and the increases of the flattening ones for the different size tubes, and the ones based on the thinning or the flattening are larger than on the

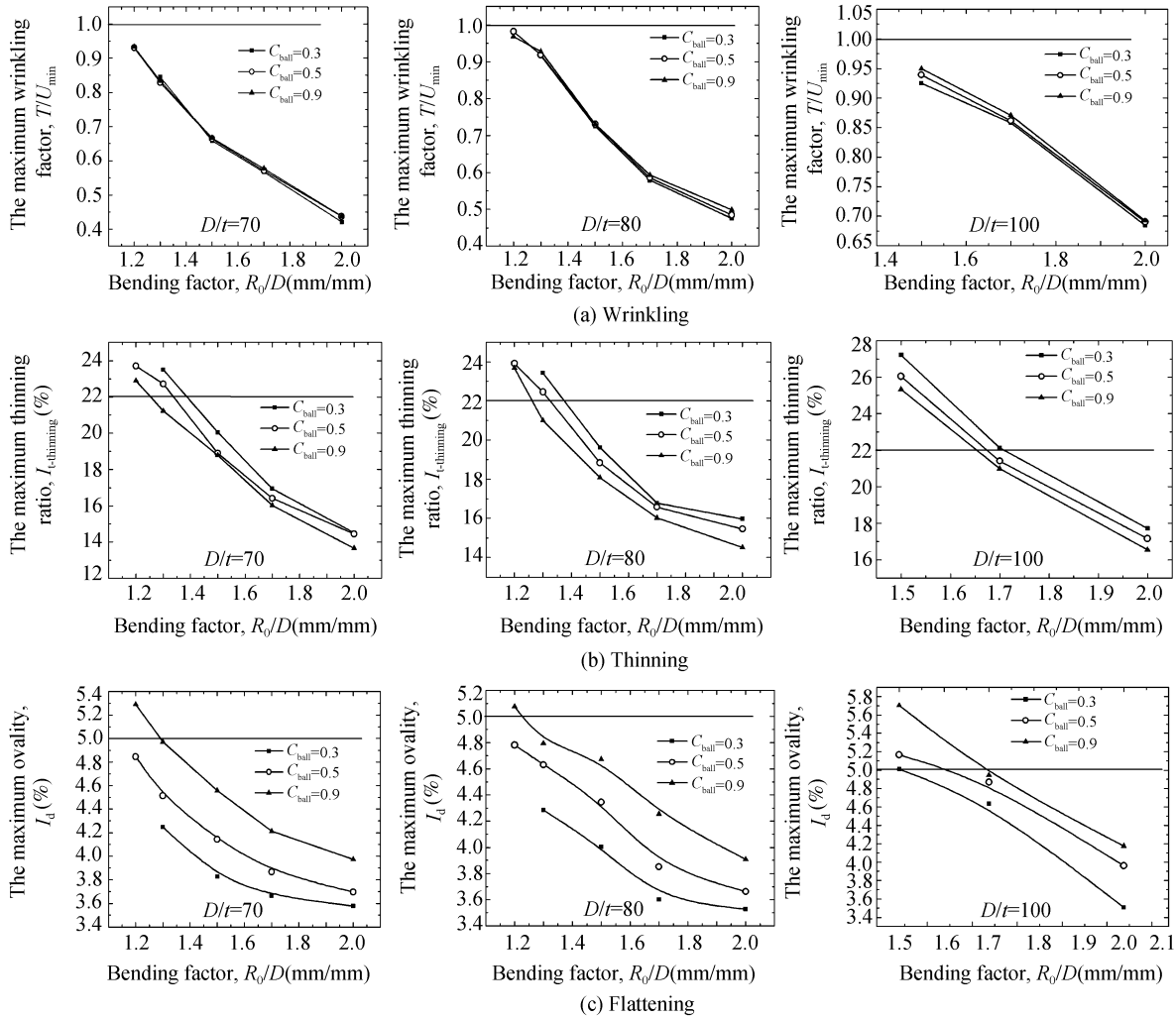

Figure 11 Effects of mandrel ball diameters on different forming indices.

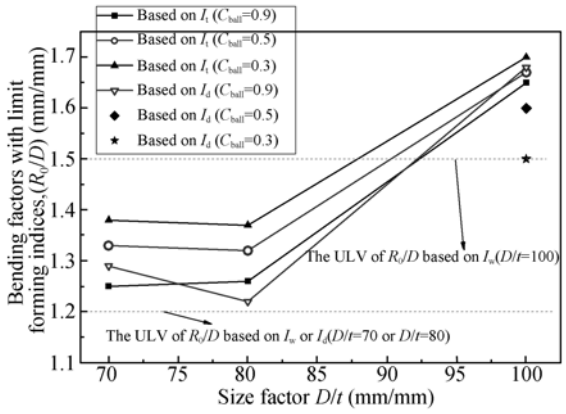

Figure 12 Effects of mandrel ball diameters on critical bending factors.

wrinkling. Thus, the tube maximum critical bending factors will be based on the thinning or flattening with decreasing the mandrel ball diameters.

3.4 Effects of ACL on critical bending factors

3.4.1 Effects of ACL on multi-indices

Due to the very large wrinkling possibility of the tube with *D*/*t* of 100 in the bending processes under the ACL, the effects of the ACL on the multi-indices under the different bending factors are studied only for the tubes with *D*/*t* of 70 and 80, as shown in Figure 13. It can be found that under the small mandrel ball thickness and diameters, the ACL will increase the tube wrinkling possibilities and decrease

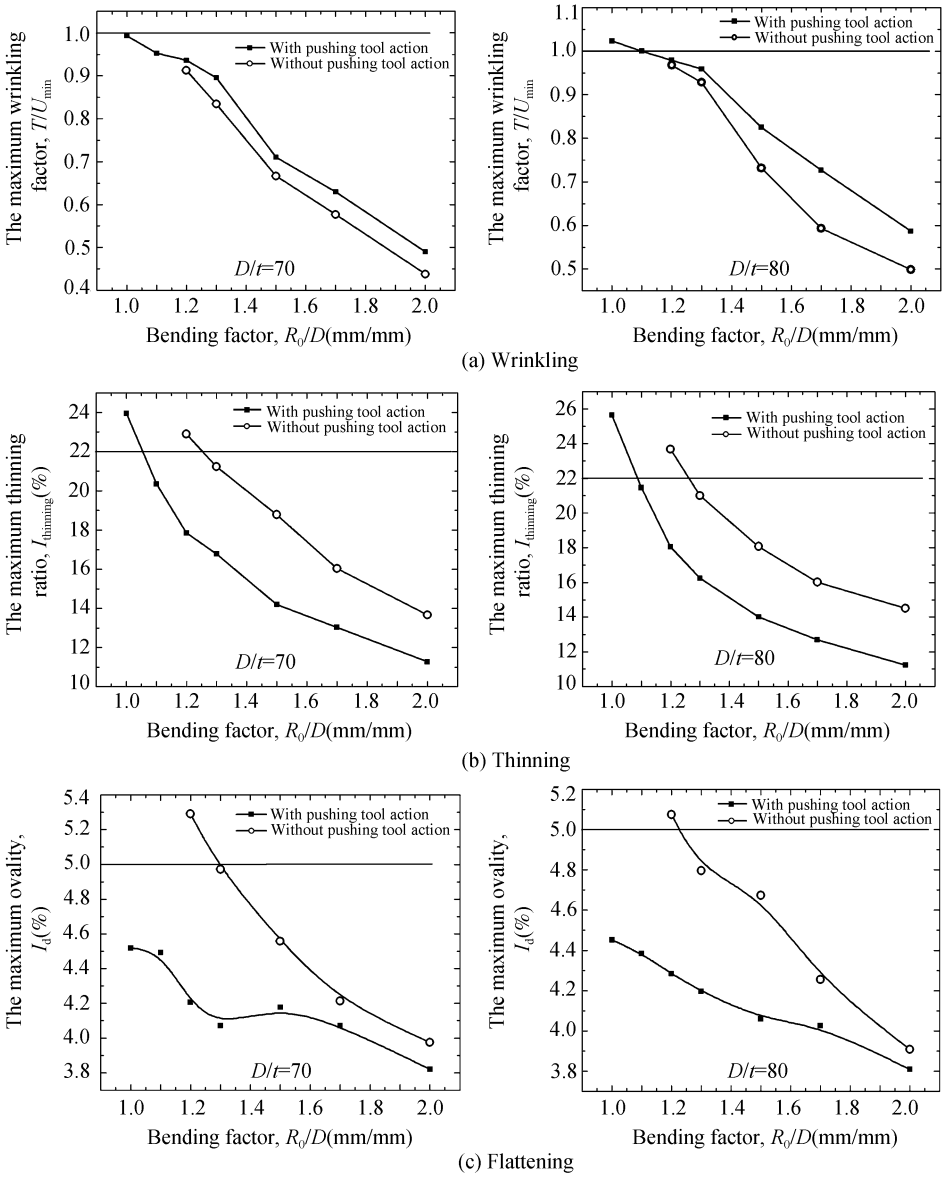

Figure 13 Effects of pushing tool on different forming indices.

both the tube thinning and flattening degrees.

3.4.2 Effects of ACL on the maximum critical bending factors

Figure 14 shows the tube critical bending factors corresponding to the ACL obtained from Figure 13. It can be found from Figure 14 that under the small mandrel ball thickness and diameters, the ACL can lead to the decreases of the critical bending factors based on the thinning and flattening and the increases of the wrinkling ones; the larger the *D*/*t*, the smaller the effects of the ACL on the thinning and flattening. For the tube with *D*/*t* of 70, the critical thinning bending factor is larger than the others, and thus the tube maximum critical bending factor is based on the thinning under the ACL. For the tube with *D*/*t* of 80, the maximum critical bending factor is based on the wrinkling under the ACL, because the tube wrinkling possibility will increase with increasing *D*/*t*.

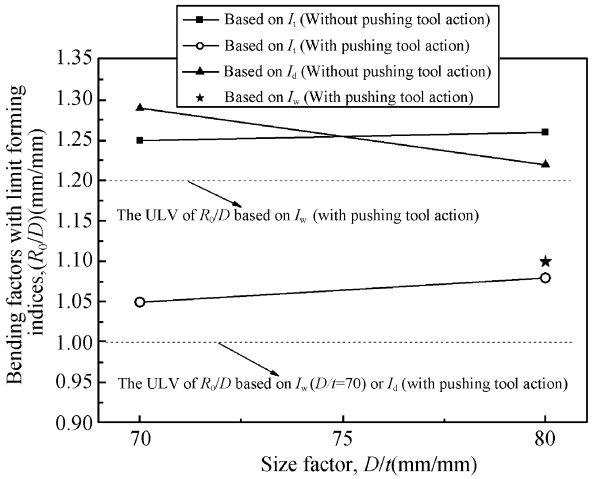

Figure 14 Effects of pushing tool on critical bending factors.

3.5 Roles of process parameters in enabling limit bending processes

Figure 15 shows the effects of the clearance and friction parameters on the maximum critical bending factors in the NC bending processes of the different size tubes. In Figure 15, the mandrel shank diameters are measured by the clearances between the mandrel shanks and the tubes. It can be found that the decreases of the mandrel shank diameters or the friction between the bending dies and the tubes will lead to the increases of the tube maximum critical bending factors and the maximum relative increment of the ones is 65.9%; the clearances have a greater influence on the ones than the friction; the larger the *D*/*t* or the mandrel ball thickness, the larger the their effects. Besides, under the large mandrel ball thickness, the tube maximum bending factors will be based on the wrinkling (Figure 8).

Figure 16 shows the effects of the mandrel ball thickness and diameters on the maximum critical bending factors under the clearance and friction parameters shown in Table 3, which enable the tube bending processes with smaller bending factors. It can be found that the decreases of the mandrel ball thickness and diameters, or the ACL under the small mandrel ball thickness and diameters will lead to the decreases of the ones enabling the tube limit bending processes. From Figures 15 and 16, it also can be found that the larger the *D*/*t*, the larger the effects of the increases of the mandrel shank diameters or the friction between the bending dies and the tubes, or the decreases of the mandrel ball thickness; the smaller the *D*/*t*, the larger the effects of the ACL and the decreases of the mandrel ball diameters.

Figure 17 shows the minimum bending factors obtained from Figure 16, which are based on the effects of the process parameter combinations on the multi-indices in these NC bending processes. It can be found that under these optimum process parameter combinations, the forming limits

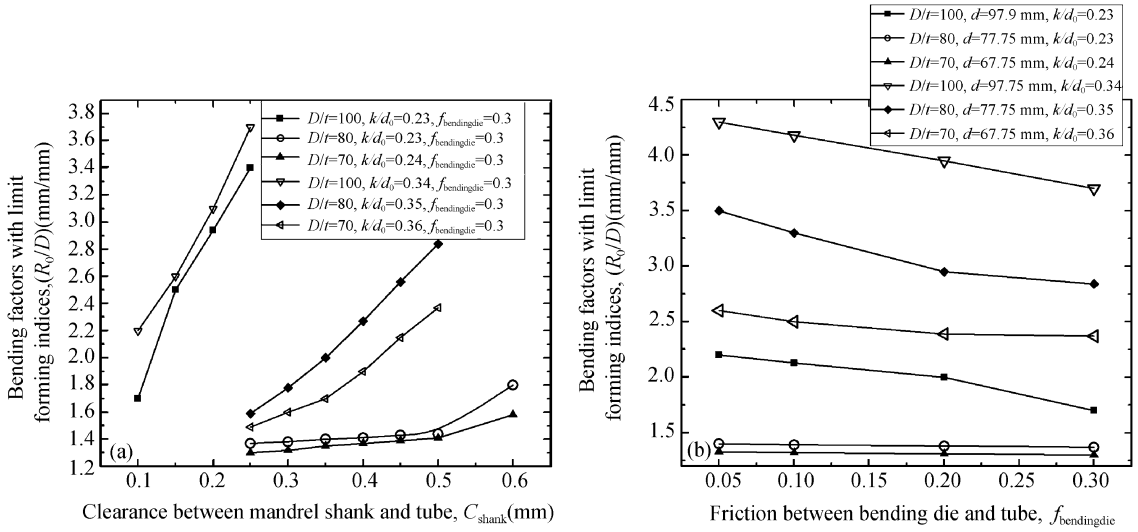

Figure 15 Effects of clearance and friction parameters on the maximum critical bending factors. (a) Clearance between mandrel shank and tube; (b) friction between bending die and tube.

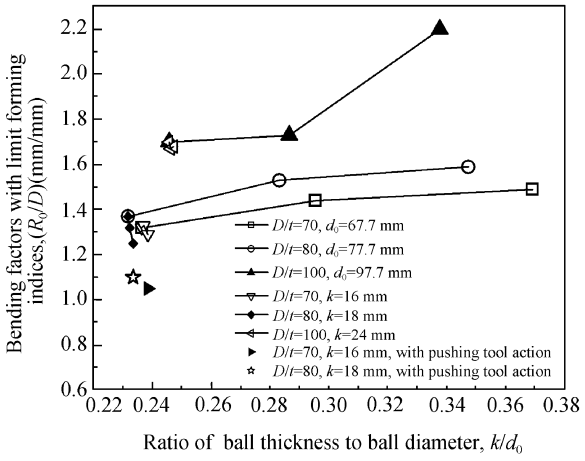

Figure 16 Effects of mandrel ball thickness and diameters on the maximum critical bending factors.

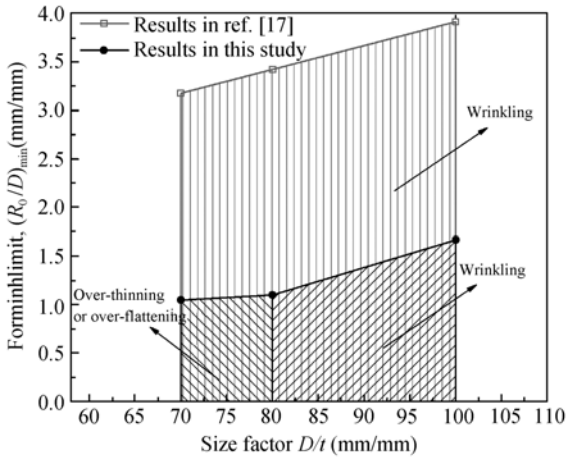

Figure 17 The minimum bending factors of different size tubes.

will be decided by the limit thinning values for the tubes with diameters<80 mm, while by the wrinkling for the tubes with diameters≥80 mm. The forming limits obtained from this method are smaller than the analytical results in ref. [17], and are reduced by 57.39%. Figure 18 shows the forming qualities in the simulation of the bending process of the tube (D/t=80) with the minimum bending factor. It can be found that the forming qualities are acceptable.

3.6 Verification of process parameter roles

In order to verify the roles of the process parameters in enabling the tube limit bending processes, a bending experiment of the tube with D=127 mm and t=1.24 mm was done. The tube material was 6061O, the material extension ratio was 26.50%.

Without considering the effect of the tube geometry size on the tube constitutive equation, the appropriate ranges of the process parameter combinations (Table 5) for the bending factor of 1.7 are obtained from the method shown in Figure 4. After decreasing the bending factor and changing process parameter combination during these appropriate ranges according to this searching algorithm of forming limits shown in Figure 5, the minimum bending factor is predicted and the value is 1.5. The optimum die parameters and friction conditions between the different dies and the tube corresponding to the minimum bending factor are also listed in Table 5.

The experiment was performed on NC tube bender W27YPC-159 (Figure 19). In this experiment, the bending die and pressure die were unlubricated, and the contacting interfaces between the tube and the wiper die and mandrel were lubricated well by the drawing oil for stainless steel S980B. These lubrication methods enabled the friction conditions between the different dies and the tube to tend toward the optimum values (Table 5). Meanwhile, with keeping the other optimum process parameters unchanged as shown in Table 5, two different mandrel parameter combinations were used respectively. As shown in Table 6, the limit bending processes were achieved successfully under these optimum process parameters and the experimental tube part is shown in Figure 20; when the process parameters deviated from the optimum ones in a small range, the tube forming qualities in the limit bending process would be bad. Thus, this searching algorithm of forming limits in this study is reliable, because the effects of process parameters

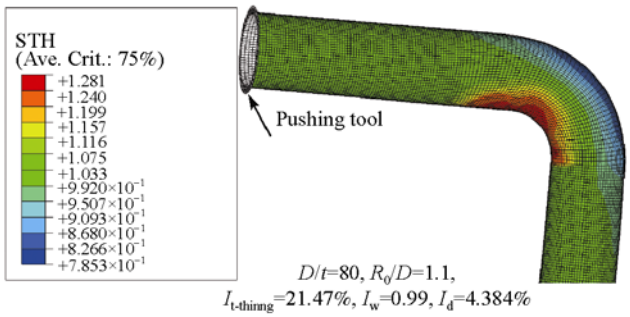

Figure 18 Tube forming qualities for the minimum bending factors.

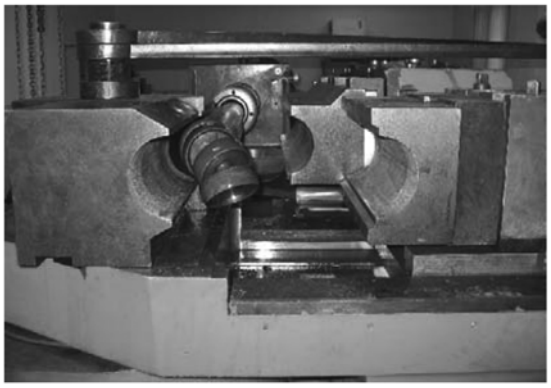

Figure 19 Illustration of experimental equipment.

Table 5 Process parameter combination ranges

Process parameters	Parameter ranges (R_0/D=1.7)	Optimum parameters (R_0/D=1.5)
Tube diameter, D (mm)	127	127
Wall thickness, t (mm)	1.24	1.24
Bending radius, R_0 (mm)	215.90	190.50
Mandrel diameter, d (mm)	124.26－124.31	124.26
Ball diameter, d_0 (mm)	123.90－124.21	123.90
Thickness of ball, k (mm)	35－40	35
No. of balls, N	3, 4	3
Extension length of mandrel, e (mm)	5－7	7
Final bending angle, θ_0 (rad)	$\pi/2$	$\pi/2$
Assembling clearance of pressure die, C_p (mm)	0.10－0.20	0.15
Assembling clearance of wiper die, C_w (mm)	0.15－0.20	0.17
Assembling clearance of bending die, C_b (mm)	0.10－0.15	0.10
Tube outside surface vs. wiper die, f_w	0.05－0.06	0.05
Tube outside surface vs. pressure die, f_p	0.25－0.30	0.30
Tube outside surface vs. bending die, f_b	0.25－0.30	0.30
Tube inside surface vs. clamping plug	0.25－0.30	0.30
Tube inside surface vs. mandrel with balls, f_m	0.05－0.07	0.05

Note: The cavity tolerance of pressure die is set as 0－0.05 mm and the ones of wiper die and bending die 0.1－0.15 mm under the bending factor of 1.7; the cavity tolerance of pressure die is set as 0 mm and the ones of wiper die and bending die 0.1 mm under the bending factor of 1.5.

Table 6 Experimental conditions and results

No.	D (mm)	d_0 (mm)	k (mm)	N	Wrinkling	I_t (%)	I_d (%)
1	124.10	124.00	45	3	Yes	30	3.5
2	124.26	123.90	35	3	No	26	3

Note: The other process parameters are the same as the ones listed in Table 5.

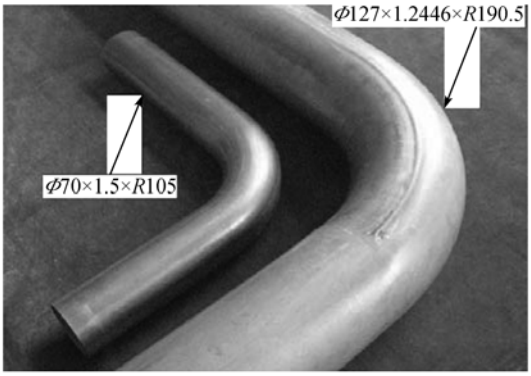

Figure 20 Parts of the experimental tubes.

on these different forming indices have been taken into consideration in this algorithm while without considering the effects of the tube geometry size on the tube constitutive equation.

4 Conclusions

A search algorithm of the forming limits is put forward based on the 3D elastic-plastic FE model and the wrinkling energy prediction model for NC bending processes of AATTs with large diameters under axial compression loading (ACL) or not. This algorithm can consider effectively effects of process parameter combinations including die, friction parameters on the multi-indices in these bending processes with smaller bending factors. Based on this algorithm, the roles of the clearances and friction between the different dies and the tubes, the mandrel ball thickness and diameters, and the ACL in enabling these limit bending processes are revealed and the forming limits of these different diameter AATTs are obtained.

1) With decreasing the mandrel shank diameters or the friction between the bending dies and the tubes, the tube maximum critical bending factors will increase and be based on the wrinkling especially under the large mandrel ball thickness. The larger the D/t or the mandrel ball thickness, the larger the effects of the mandrel shank diameters and friction between the bending dies and the tubes.

2) Within the appropriate ranges of friction and clearances between the different dies and the tubes enabling the tube bending processes with smaller bending factors, the decreases of the mandrel ball thickness or diameters, or the ACL under the small mandrel ball thickness and diameters will lead to the decrease of the maximum critical bending factors enabling the tube limit bending processes. The larger the D/t, the larger the effects of the mandrel ball thickness; the smaller the D/t, the larger the effects of the mandrel ball diameters and the ACL.

3) Without considering the effects of the tube geometry sizes on the tube constitutive equations and under these op-

timum process parameter combinations, the forming limits will be decided by the limit thinning values for the tubes with diameters<80 mm, and by the wrinkling for the tubes with diameters≥80 mm. The forming limits obtained from the method in this paper are smaller than the analytical results, and are reduced by 57.39%.

4) The roles of the process parameter combinations in enabling the tube limit bending processes are verified by experimental results. The limit bending experiment of the large size tube (D/t=100) has been accomplished successfully.

The achievements in this study provide a scientific base for the understanding and prediction of forming limits of AATTs with large diameters and the control of these limit tube bending processes.

This work was supported by the National Natural Science Foundation of China (Grant Nos. 59975076, 50175092, 50905144) and the National Science Found of China for Distinguished Young Scholars (Grant No. 50225518).

1 Yang H, Sun Z C, Lin Y, et al. Advanced plastic processing technology and research progress on tube forming (in Chinese). J Plast Eng, 2001, 8(2): 86–88
2 Gillanders J. Pipe and Tube Bending Mannual. Houston: Gulf Publishing Company, 1984. 102
3 Butuca M C, Gracioa J J, Barata da R A. An experimental and theoretical analysis on the application of stress-based forming limit criterion. Int J Mech Sci, 2006, 48(4): 414–429
4 Ozturk F, Lee D. Analysis of forming limits using ductile fracture criteria. J Mater Process Technol, 2004, 147(3): 397–404
5 Koc M, Altan T. Prediction of forming limits and parameters in the tube hydroforming process. Int J Mach Tools Manuf, 2002, 42(1): 123–138
6 Wang X, Cao J. Wrinkling limit in tube bending. Trans ASME, 2001, 123(4): 430–435
7 Yang H, Lin Y. Wrinkling analysis for forming limit of tube bending processes. J Mater Process Technol, 2004, 152(3): 363–369
8 Li H, Yang H, Zhan M, et al. A new method to accurately obtain wrinkling limit diagram in NC bending process of thin-walled tube with large diameter under different loading paths. J Mater Process Technol, 2006, 177(1-3): 192–196
9 Narayanasamy R, Loganathan C. Study on wrinkling limit of commercially pure aluminum sheet metals of different grades when drawn through conical and tractrix dies. Mater Sci Eng A, 2006, 419(1-2): 249–261
10 Palumbo G, Tricarico L. Numerical and experimental investigations on the warm deep drawing process of circular aluminum alloy specimens. J Mater Process Technol, 2007, 184(1-3): 115–123
11 Yang T S. The strain path and forming limit analysis of the lubricated sheet metal forming process. Int J Mach Tools Manuf, 2007, 47(7-8): 1311–1321
12 Kima J, Kimb S W, Songa W J, et al. Analytical and numerical approach to prediction of forming limit in tube hydroforming. Int J Mech Sci, 2005, 47(7): 1023–1037
13 Lee J W, Kwon H C, Rhee M H, et al. Determination of forming limit of a structural aluminum tube in rubber pad bending. J Mater Process Technol, 2003, 140(1-3): 487–493
14 Li H, Yang H, Zhan M, et al. Wrinkling limit based on FEM virtual experiment during NC bending process of thin-walled tube. Mater Sci Forum, 2004, 471-472: 498–502
15 Gu R J, Yang H, Zhan M, et al. Effect of mandrel on cross section quality of thin-walled tube NC bending. Trans Nonferrous Met Soc China, 2005, 15(6): 1264–1274
16 Li H, Yang H, Zhan M, et al. Forming characteristics of thin-walled tube bending process with small bending radius. Trans Nonferrous Met Soc China, 2006, 16(Suppl): 613–623
17 Li H. Study on wrinkling behaviors under multi-die constraints in thin-walled tube NC bending (in Chinese). Dissertation of Doctoral Degree. Xi'an: Northwestern Polytechnical University, 2007. 76
18 Yang H, Yan J, Zhan M, et al. 3D numerical study on wrinkling characteristics in NC bending of aluminum alloy thin-walled tubes with large diameters under multi-die constraints. Comput Mater Sci, 2009, 45(4): 1052–1067
19 ABAQUS. Version 6.5. Washington (FL): Hibbit Karlson and Sorensen Inc. 2005
20 Sun W Y, Xu C X, Zhu D T, et al. Optimization Method (in Chinese). Beijing: Higher Education Press, 2004. 89